ELSEVIER

S0032-3861(96)00154-1

Polymer Vol. 37 No. 16, pp. 3483–3491, 1996

0032-3861/96/$15.00 + 0.00

polymer papers

A new Brillouin scattering analysis of high frequency relaxations in liquids demonstrated at the hypersound relaxation of PPG

H. H. Krbecek, W. Kupisch and M. Pietralla*
Abteilung für Experimentelle Physik, Universität Ulm, 89069 Ulm, Germany
(Received 3 January 1995; revised 6 December 1995)

We present a new method to analyse data obtained by Brillouin scattering. Using two scattering geometries simultaneously and measuring separately the refractive index $n(T)$ we can determine the logarithmic derivative $\partial \lg M'(\omega, T)/\partial \lg \omega = Q_M$ and thus are able to characterize unambiguously the dominant fast processes by high precision frequency shift measurements. For a sufficient narrow relaxation time distribution the imaginary part $M''(\omega, T)$ of the complex modulus $M(\omega, T) = M'(\omega, T) + i\mathrm{M}''(\omega, T)$ can be derived. Analysing data of poly(propylene glycol) with $M_w = 1000$ (PPG 1000) we find the fastest process to show Arrhenius behaviour. Using published data from impulsive surface scattering we can finally deconvolute a set of three different processes: two exhibiting Arrhenius behaviour and one showing Vogel–Fulcher–Tammann behaviour. These three processes describe the data to a high accuracy and are tentatively assigned to molecular motions. At high frequencies the relaxation time distribution observed narrows to a single relaxation time. In the light of these results it seems questionable to use linewidth data from Brillouin scattering experiments to determine the width of the relaxation process. From the present work we believe the experiments with surface acoustic waves to be the most effective since they can be coupled with Brillouin scattering experiments. Copyright © 1996 Elsevier Science Ltd.

(Keywords: poly(propylene glycol); relaxation map; relaxation processes; hypersound; Brillouin scattering)

INTRODUCTION

Investigations of relaxational phenomena in oligomeric liquids help to understand the molecular dynamics in complex fluids. The whole step in the complex modulus $M(\omega) = M'(\omega) + iM''(\omega)$, as a function of the frequency ω, should be covered by the measurements, which is often impossible. Results obtained by different methods, such as photon correlation spectroscopy (PCS)[1], ultrasound[2,3] or Brillouin scattering (BS)[4,5] are plotted to one relaxation map. Brillouin spectroscopy provides the information about the highest frequencies in a very restricted range beyond about 1 GHz. Temperature variations are used to explore the relaxation process and sometimes it is possible to cross the transition region[6], as in the case of poly(propylene glycol) (PPG) which reveals a secondary relaxation around room temperature, irrespective of molecular weight[4]. It is usual to measure the lineshift and the linewidth of the phonon lines. The former is transformed to the real part of the longitudinal modulus

$$M'(\omega) = K'(\omega) + \frac{4}{3}G'(\omega) \qquad (1)$$

with $K'(\omega)$, $G'(\omega)$ are the real part of the complex bulk modulus $K(\omega)$ and the complex shear modulus $G(\omega)$ respectively. The linewidth Γq^2 represents the acoustic damping (Γ is the damping constant). These quantities are compared to theoretical expressions of hydrodynamic theories[4]. The agreement is questionable if only part of the relaxation process is covered by the experiment[7]. One of the main problems is to determine $v_\infty(T) = v(T, \omega \to \infty)$[3–5]. Evaluating the linewidth involves great errors, compared to the accuracy of the lineshift. A controversy in interpreting data obtained from *n*-alkane melts[7–9] motivated us to search for a method to detect unambiguously hypersonic frequency dispersion from Brillouin scattering without using theoretical models. In fact such a method exists and has been assigned the opto-acoustic dispersion function[10]. It is based on simultaneous measurement of Brillouin lineshifts belonging to two different scattering geometries, i.e. to two different $\vec{q}$-vectors and a separate measurement of the refractive index n. The sensitivity is very high and the method is well adapted for very weak processes. We used PPG, with its well-known dispersion, as a test substance. Well-known does not mean well understood, which is shown by the controversial interpretation of the data obtained[11,12]. Our interest was to incorporate relaxation models into the data treatment to see whether this controversy can be resolved.

BRILLOUIN SCATTERING AND HYPERSOUND RELAXATION: METHODICAL BACKGROUND

Brillouin scattering is the inelastic scattering of light by

* To whom correspondence should be addressed

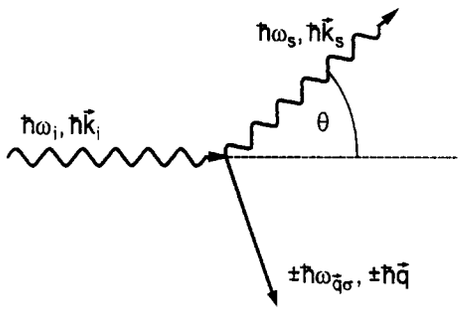

Figure 1 Kinematic of the Brillouin scattering process: an incident photon (energy $\epsilon_i = \hbar\omega_i$, momentum $\vec{p}_i = \hbar\vec{k}_i$) interacts with a phonon ($\epsilon_{\vec{q}\sigma} = \hbar\omega_{\vec{q}\sigma}$, $\vec{p} = \hbar\vec{q}$) and a scattered photon results with different momentum $\vec{p}_s = \hbar\vec{k}_s$ and slightly different energy $\epsilon_s = \hbar\omega_s$. Where ω_i, ω_s, $\omega_{\vec{q}\sigma}$ are radian frequencies, $\vec{k}_i$, $\vec{k}_s$, $\vec{q}$ are wave vectors of the corresponding quantum and σ is the polarization index of the phonon

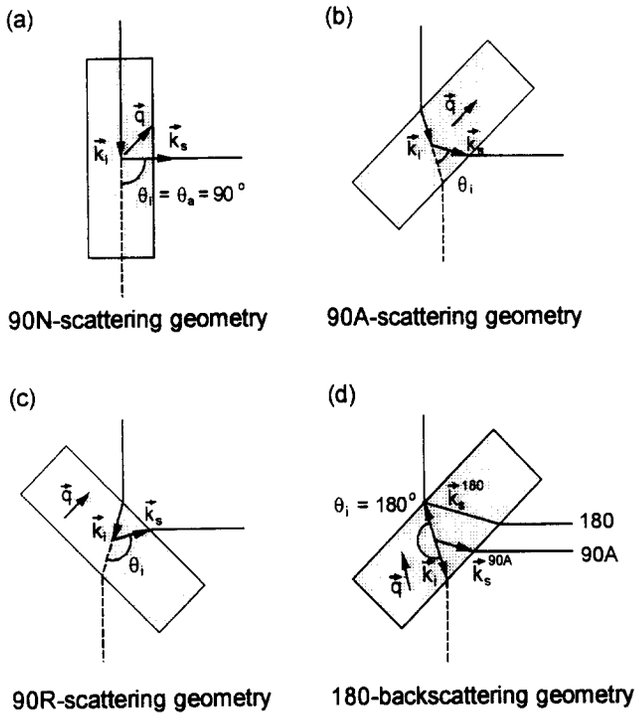

Figure 2 Standard scattering geometries with fixed outer scattering angle $\theta_a = 90°$ differing from the inner scattering angle θ_i: (a) 90**N**ormal-, (b) 90**A**ntireflection-, (c) 90**R**eflection- and (d) 180-back-scattering geometry

thermally excited sound waves in solids and liquids. For details see for example references 13 and 14. The energy and momentum conservation is described by a three quantum process (*Figure 1*). The frequency shift $\Delta\omega$ of the scattered photon is given by

$$\Delta\omega = \omega_{\vec{q}\sigma} = |\omega_s - \omega_i| = 2 \cdot \omega_i \cdot \frac{V_{\vec{q}\sigma}}{c/n} \cdot \sin\frac{\theta}{2} \qquad (2)$$

where $v_{\vec{q}\sigma}$ is the sound velocity related to the elastic modulus, $M_{\vec{q}\sigma}$ and the mass density ρ by $v_{\vec{q}\sigma} = \{M_{\vec{q}\sigma}/\rho\}^{1,2}$; n is the optical refractive index and c the velocity of light in vacuum. The standard scattering geometries are shown in *Figure 2*. The outer scattering angle θ_a is fixed to 90° and differs from the inner scattering angle θ_i. The absolute value $q = 2\pi/\Lambda$ (Λ is acoustic wavelength) of the wave vector $\vec{q}$ is correlated with the inner scattering angle by $q = |\vec{q}| = 2 \cdot |\vec{k}_i| \cdot \sin\theta_i/2$. For a given scattering geometry the sound velocity v (index $\vec{q}\sigma$ suppressed) can be calculated from the measured frequency shift $\Delta\nu = \Delta\omega/2\pi$ by using equations (3a)–(3d), which follow directly from equation (2).

$$90N: \quad v = \frac{\Delta\nu_{90N}\lambda_0}{\sqrt{2}n} \qquad (3a)$$

$$90A: \quad v = \frac{\Delta\nu_{90A}\lambda_0}{\sqrt{2}} \qquad (3b)$$

$$90R: \quad v = \frac{\Delta\nu_{90R}\lambda_0}{\sqrt{4n^2 - 2}} \qquad (3c)$$

$$180: \quad v = \frac{\Delta\nu_{180}\lambda_0}{2n}, \qquad (3d)$$

where λ_0 is the vacuum wavelength of the incident laser light. The symmetrical 90A-geometry not involving the refractive index n should be favoured. In combination with another scattering geometry it enables determination of the refractive index if acoustic dispersion can be neglected. The combination $90A/90R$ can be done simultaneously on the same sample volume at the same temperature, cf. *Figure 3*. If acoustic dispersion is present, $n(T)$ which must be known from independent measurements will not be reproduced. This leads to a very sensitive method to detect relaxation processes in the region of interest. The method was first introduced by Krüger *et al.*[8,10]. Equations (3a)–(3d) yield the following definition of the opto-acoustic dispersion function $D_X(T)$*[15]:

$$D_{90N}(T) = \frac{\Delta\nu_{90N}(T)}{\Delta\nu_{90A}(T)} \qquad (4a)$$

$$D_{180}(T) = \frac{1}{\sqrt{2}}\frac{\Delta\nu_{180}(T)}{\Delta\nu_{90A}(T)} \qquad (4b)$$

$$D_{90R}(T) = \sqrt{\frac{1}{2}\left[1 + \left(\frac{\Delta\nu_{90R}(T)}{\Delta\nu_{90A}(T)}\right)^2\right]} \qquad (4c)$$

Without acoustic dispersion, i.e. $\omega\tau \ll 1$ or $\omega\tau \gg 1$ (τ is relaxation time) $D_X(T) = n(T)$ holds, whereas a weak frequency-dependence of the modulus leads to a distinct deviation from the refractive index $n(T)$. The D-function can be determined with great accuracy by Brillouin spectroscopy because only the ratio of two frequency shifts is involved. Thus the D-function is independent of the calibration of the spectrometer. The accuracy is governed by the constancy of temperature.

The D-function has an inclined co-ordinate system given by the refractive index n as a function of

* In ref. 10 a generalized formulation of the opto-acoustic dispersion function $D_X(T)$ for the combination of the $90A$-scattering geometry with any other scattering geometry X (inner scattering angle θ_X) is given, which can be easily derived from equation (2):

$$D_X(T) = n(T)\sqrt{\frac{M'_X(T)}{M'_{90A}(T)}} = \frac{1}{\sqrt{2}\sin\frac{\theta_X(T)}{2}}\frac{\Delta\nu_X(T)}{\Delta\nu_{90A}(T)}$$

For $X = 90N$ and $X = 180$ this expression is equal to equation (4a)–(4b), but not equal to equation (4c) for $X = 90R$. The latter is only equal in the range of no acoustic dispersion

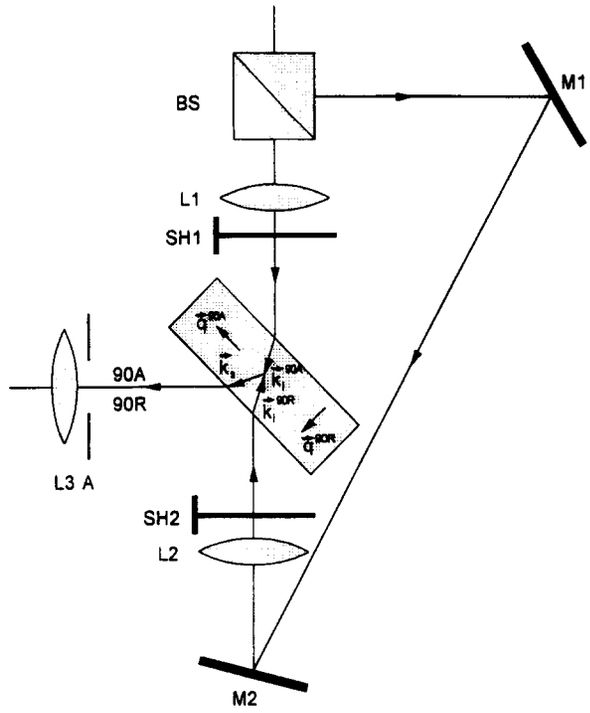

Figure 3 90*A*/90*R*-double geometry: the Brillouin frequency shifts are measured quasi-simultaneously on the same sample volume. Using Shutter SH1 and SH2 each of both scattering geometries can be easily selected. Switching back and forth is done computer controlled synchronously with changing the data accumulation area of the multichannel analyser. A, aperture; BS, beam-splitter; L, lens; M, mirror; SH, shutter

temperature. A rectangular system is given by $R_X(T)$ the ratio of the moduli belonging to the two different frequencies of the *X*- and the 90*A*-geometries. In case of the 90A/90R combination we get

$$R = \frac{M'(\nu_{90R}, T)}{M'(\nu_{90A}, T)} = \left(\frac{\nu_{90R}}{\nu_{90A}}\right)^2 \frac{1}{2n^2 - 1} \tag{5}$$

$R > 1$ indicates the appearance of a mechanical relaxation process. The 90*A*/90*R*-arrangement shows a high sensitivity since only lineshifts and the refractive index are measured with an accuracy of $\Delta\nu < \pm 0.1\%$ and an accuracy of $n < \pm 0.25\%$ respectively, such that a 1% dispersion of the modulus is easily detected. This representation is free of any model for the frequency and temperature dependence of the modulus.

We now introduce an alternative representation. Two frequencies differing by a factor of about two provide the possibility to determine a difference quotient which for slowly varying functions is just the derivative

$$Q_M(T) = \frac{\partial \lg M'(\omega, T)}{\partial \lg \omega} \approx \frac{\bar{\omega}}{\bar{M}'} \frac{\Delta M'}{\Delta \omega} \tag{6}$$

where $\Delta M'$ and $\Delta\omega$ are the differences, and $\bar{M}'$ and $\bar{\omega}$ the average values of the corresponding variables. By simultaneously detecting two scattering geometries and varying the temperature T a frequency window of the width $\Delta\omega$ is shifted over the curve $M(\omega, T)$, as shown in *Figure 4*. In doing so we use the temperature–frequency superposition principle, according to which varying the temperature is equivalent to varying the frequency and *vice versa*. In Brillouin spectroscopy two wave vectors of different magnitude are selected. Their frequencies

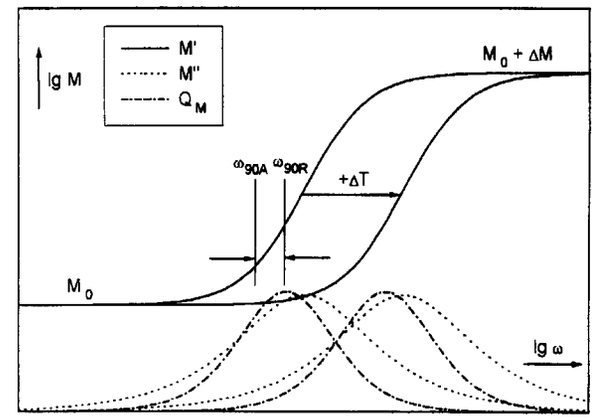

Figure 4 The Q_M function can be directly obtained from the Brillouin double scattering geometry. For a Debye process it can be converted to the loss modulus. By varying the temperature a frequency window of the width $\Delta\omega$ is shifted over the curve $M(\omega, T) = M'(\omega, T) + i \cdot M''(\omega, T)$

follow from the dispersion relation. Therefore the width of the frequency window can vary slightly.

The real part of the moduli can be expressed by

$$M'(\omega_{90A}, T) = \rho(T) \frac{\omega_{90A}^2(T)}{q_{90A}^2} \tag{7a}$$

$$M'(\omega_{90R}, T) = \rho(T) \frac{\omega_{90R}^2(T)}{q_{90R}^2(T)} \tag{7b}$$

where q_{90A} is independent of temperature. The density $\rho(T)$ as a function of temperature can be obtained by using the Lorentz–Lorenz equation

$$\frac{n^2(T) - 1}{n^2(T) + 2} = r\rho(T) \tag{8}$$

The specific refractivity r is almost independent of temperature. We obtain for the difference $\Delta M'(T) = M'(\omega_{90R}, T) - M'(\omega_{90A}, T)$ of the moduli

$$\Delta M' = \frac{\lambda_0^2}{2r} \frac{n^2 - 1}{n^2 + 2} \left\{ \frac{\nu_{90R}^2}{2n^2 - 1} - \nu_{90A}^2 \right\} \tag{9}$$

and for the average value $\bar{M}'(T) = [M'(\omega_{90R}, T) + M'(\omega_{90A}, T)]/2$

$$\bar{M}' = \frac{\lambda_0^2 n^2 - 1}{4r n^2 + 2} \left\{ \frac{\nu_{90R}^2}{2n^2 - 1} + \nu_{90A}^2 \right\} \tag{10}$$

For clarity the variable T has been suppressed. Finally we get with equation (6)

$$Q_M = \left\{ 1 + 2\left[\frac{\nu_{90R}}{\nu_{90A}} - 1 \right]^{-1} \right\} \cdot \left\{ 1 - 2\left[\left(\frac{\nu_{90R}}{\nu_{90A}} \right)^2 \frac{1}{2n^2 - 1} + 1 \right]^{-1} \right\} \tag{11}$$

Like the opto-acoustic dispersion function $Q_M(T)$ can be determined with high relative accuracy on the same reasons. The uncertainty of the refractive index has negligible influence on the accuracy. $Q_M(T)$ is experimentally determined as a function of temperature with a slowly varying average frequency (*Figure 4*) and up to

this point free of model assumptions. If a theory delivers an expression for $M(\omega, T)$ it can be compared directly to the experiment if the measured frequencies are inserted.

The time-dependence of a modulus $M(t)$ can be written as

$$M(t) = M_0 + \int_{-\infty}^{+\infty} H(\tau) e^{-t/\tau} d\ln\tau \qquad (12)$$

which for a dynamic load transforms to

$$M'(\omega) = M_0 + \int_{-\infty}^{+\infty} H(\tau) \frac{\omega^2\tau^2}{1+\omega^2\tau^2} d\ln\tau \qquad (13a)$$

$$M''(\omega) = \int_{-\infty}^{+\infty} H(\tau) \frac{\omega\tau}{1+\omega^2\tau^2} d\ln\tau \qquad (13b)$$

The fraction is the Debye relaxation function. The relaxation time distribution $H(\tau)$ is generally difficult, sometimes impossible, to obtain and parametric representations of $M(\omega)$ are widely used. For a sufficiently steep change in $M(\omega)$ to a first approximation the relation

$$H(\tau = 1/\omega) = \frac{dM'(\omega)}{d\ln\omega} = M'(\omega) \cdot Q_M(\omega) \qquad (14)$$

is valid[16]. For the Debye relaxation function we can determine $M''(\omega)$ from the Q_M-function via

$$M''(\omega) = \sqrt{\frac{\Delta M}{2} M'(\omega) \cdot Q_M(\omega)} \qquad (15)$$

where $\Delta M = M_\infty - M_0$ is the relaxation strength of the Debye process. Equation (15) may approximately be used also for other relaxation functions. The $\alpha\beta$-relaxator of Havriliak–Negami[17]

$$M(\omega) = M_\infty - \Delta M \frac{1}{(1+(i\omega\tau)^\alpha)^\beta} \qquad (16)$$

embraces the Debye case ($\alpha = 1$, $\beta = 1$), the Cole–Cole case ($\beta = 1$)[18] and the Davidson–Cole case ($\alpha = 1$)[19]. All these variations of the Debye relaxator have a wider spectral range.

The temperature dependence of the modulus and the relaxation time lead to the temperature–frequency or temperature–time superposition principle respectively which for thermorheological simple fluids with x as reduced variable reads as follows:

$$M(\lg\omega, T) = M(x) \quad \text{with} \quad x = \lg\omega - \lg a_T \qquad (17)$$

The temperature dependent shift factor $a_T = \omega/\omega_R$ is determined by the ratio of the frequency ω at temperature T and the frequency ω_R at reference temperature T_R. It involves the shift factor a'_T and $\lg a'_T = -\lg a_T$. The temperature dependence of the shift factor a_T can be expressed by

$$\lg a_T = \frac{C_1(T - T_R)}{C_2 + (T - T_R)} \qquad (18)$$

the generalized WLF-equation[20]. It is used to construct the whole relaxation by superposing shifted spectra obtained in limited frequency and temperature ranges. Setting $T^* = T_R - C_2$ and $A = \ln 10 \cdot C_1 \cdot C_2$ we get the Vogel–Fulcher–Tammann (VFT) expression for the relaxation time as function of temperature

$$\tau = \tau_0 e^{\frac{A}{T - T^*}} \qquad (19)$$

With $T^* = 0$ and $A = U_0/k_B = \bar{U}_0/R$ (U_0 is the activation energy, $\bar{U}_0$ is the activation energy per mole, k_B is the Boltzmann constant, R is the molar gas constant). Equation (19) reduces to the famous Arrhenius equation of simple fluids.

EXPERIMENTAL

Sample preparation

The PPG was purchased from Aldrich as poly(1,2-propanediol) $M_W = 1000$, $\rho(25°C) = 1.005\,g\,cm^{-3}$, glass transition temperature (T_g) $\approx 190\,K$[21]. Initial experiments with the substance as received suffered from problems in the reproducibility of the refractive index. Assigning this to a changing water content we then prepared samples by drying them for at least 4 days over a molecular sieve with pore diameter 0.4 nm. Subsequently the samples were filled into sealed cuvettes. All data presented are from these dried materials.

Index of refraction

The index of refraction was measured in the range 310–430 K with an Abbé refractometer (model B from Zeiss) calibrated for 546 nm. The measured values were corrected for 514.5 nm using a table received from the manufacturer. The original thermometer was replaced by a Pt-100 resistor. The refractive index is linear in the temperature range covered: $n(T) = 1.55187 - 3.3272 \cdot 10^{-4}\,T\,K^{-1}$. It has been extrapolated to lower temperatures. From the density $\rho(25°C)$ the specific refractivity was computed using equation (8): $r = 0.26879\,cm^{-3}\,g^{-1}$.

Temperature control

For the scattering experiment at high temperatures the cuvettes were placed into a symmetrical oven to avoid thermal gradients at the sample site. Two Pt-100 resistors were used for temperature control, one connected to a high precision temperature indicator (model S 1220 from Systemteknik, Sweden), the other one to a home-built temperature controller, both with four point technique. At the sample site the temperature measurement was performed by using a Fe-constantan thermocouple with a MAWI-therm 206. At low temperatures we used an Oxford optical cryostat CF 1204 (helium flow cryostat) with an ITC 4 PID-temperature controller. Temperature control and measurement were done by two Fe/Rh resistors, one at the sample site. For both arrangements the relative temperature accuracy and temperature stability is better than ±0.1 K. The temperature ranges of the two systems overlapped in the range 300–350 K with the data in very good agreement.

Spectrometer and spectra recording

The Fabry–Perot interferometer (FPI) (Burleigh RC 110) runs with a self-built stabilization system. The scan duration for two free spectral ranges is about 0.7 s. When investigating liquids it is used in the 3-pass option, but can be changed quickly to a 5-pass option. For details cf. ref. 22. To overcome the problem of line overlapping we used the arrangement shown in *Figure 3*. After temperature equilibration every 10 scans the geometry was switched automatically to the other one, providing a quasi-simultaneous data accumulation of 500 scans in each of the two different scattering geometries. The shutters SH1 and SH2 are computer-actuated. The scattering arrangement is tested by collecting data from

pure water. Due to the absence of dispersion[23] the refractive index must be reproduced as well as the sound velocities both of which are known to a high accuracy[24–26]. In this way we are able firstly to calibrate the free spectral range to an accuracy better than ±0.1% and secondly to control exactly how the scattering geometries gave information of the same volume element of the sample.

Data evaluation

The detected Brillouin spectrum $S(\omega)$ is the convolution of the true spectrum $I(\omega)$ with the profile $L(\omega)$ of the laser line and the instrumental function $A(\omega)$.

The true spectrum $I(\omega)$ can be derived from $S(\omega)$ by deconvolution. For a single-mode laser $L(\omega) = \delta(\omega)$. The instrumental function is governed by the Airy function

$$S(\omega) = \int_{-\infty}^{+\infty} A(\omega - \omega') \int_{-\infty}^{+\infty} L(\omega'') I(\omega' - \omega'') d\omega'' d\omega' \quad (20)$$

By reason of better numerical handling near a maximum at ω_0 the sine in the Airy function may be expanded and we obtain

$$A(\omega) = \frac{A_0}{\left(1 + \dfrac{(\omega - \omega_0)^2}{\delta_{1/2}^2}(2^{1/p} - 1)\right)^p} \quad (21)$$

where A_0 is the transmission maximum, $\delta_{1/2}$ is the instrumental half-width (half-width at half-height) and p is the number of passes through the FPI. $A(\omega)$ is a function of type Pearson VII, and p is called the Pearson factor. The convolution integral (20) can be extremely complicated. Since $I(\omega)$ can be assumed to be nearly Lorentzian the convoluted spectrum $S(\omega) = I(\omega) \otimes A(\omega)$ may be approximated in good agreement again by a Pearson function, with different p and different half-width. If no quasistatic light scattering is present, the lineshape of the instrumental function dominates the Rayleigh line and p directly corresponds to the pass number. Deviations from the experimental pass number give information about the multipass quality of the interferometer. Generally the Pearson factors of each Brillouin line and of the Rayleigh line are different. Computations show that the lineshape fitted has negligible influence on the lineshift. Hence we used Pearson functions as fit functions. The nonlinear fitting procedure is based on the method of least squares[28]. All data collected from two free spectral ranges are fitted simultaneously. Thereafter the average value of the lineshifts and the linewidths are calculated.

RESULTS

In the 90A/90R-geometry spectra of PPG 1000 were recorded in the temperature range from 185 K to 465 K. From the frequency shifts the sound velocities were calculated (90A-geometry via equation (3b), 90*R*-scattering geometry via equation (3c) including the separately measured refractive index). The density $\rho(T)$ was derived from $n(T)$ making use of equation (8). Thus the moduli of both scattering geometries could be computed cf. *Figure 5*. The curves are similar to those given in reference 5 for a smaller temperature range. They cannot be directly compared, because the authors

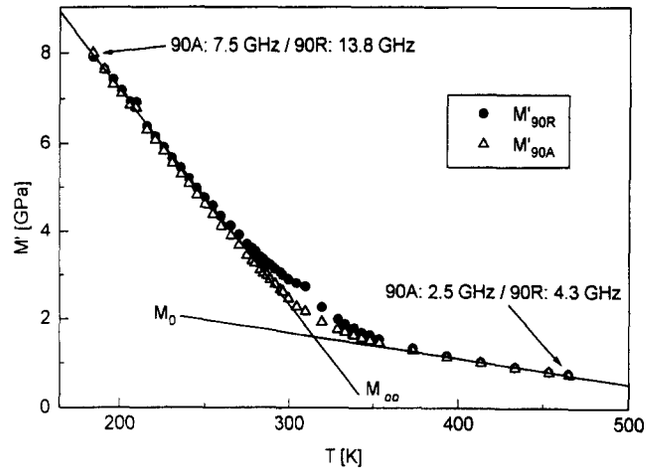

Figure 4 Real part M' of the elastic modulus in PPG 1000 as a function of temperature T, derived from Brillouin scattering measurements. Two different scattering geometries were used ($\Delta\nu_{90A} < \Delta\nu_{90R}$). The frequency range covered extends from 2.5 GHz to 7.5 GHz for the 90*A*-scattering geometry and from 4.3 GHz to 13.8 GHz for the 90*R*-scattering geometry. From the high temperature range of the 90*A*-scattering geometry we get $M_0 = (3.418 - 5.79 \cdot 10^{-3} \cdot T\,\mathrm{K}^{-1})$ GPa and from the low temperature range of the 90*R*-scattering geometry $M_\infty = (16.969 - 4.885 \cdot 10^{-2} \cdot T\,\mathrm{K}^{-1})$ GPa

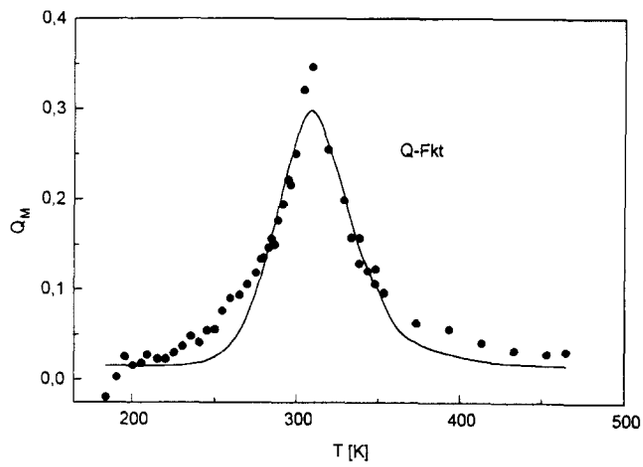

Figure 6 Q_M-function of PPG 1000 showing a relaxation process with a maximum at (309 ± 3) K at a frequency $\bar{\nu} = 6.1$ GHz

used a 90*N*-geometry leading to different frequency shifts ($\Delta\nu_{90A} < \Delta\nu_{90N} < \Delta\nu_{90R}$) and therefore to different moduli if dispersion is present. The usual interpretation requires the knowledge of the asymptotic values $M_0 = M(\nu \to 0)$ and $M_\infty = M(\nu \to \infty)$. From the high temperature range of the 90*A*-geometry we get $M_0 = (3.418 - 5.79 \cdot 10^{-3} \cdot T\,\mathrm{K}^{-1})$ GPa and from the low temperature range of the 90*R*-geometry $M_\infty = (16.969 - 4.885 \cdot 10^{-2} \cdot T\,\mathrm{K}^{-1})$ GPa. Comparing our results with the data published by Huang and Wang[21] and by Börjesson *et al.*[5] show a somewhat different temperature dependence of M_0 but a striking difference in the value of M_∞, which we assign to the water content of the samples. Exact values of M_0 and M_∞ are an essential problem of the commonly performed method.

The Q_M-function obtained from the data is depicted in *Figure 6*. The relaxation maximum at (309 ± 3) K at a frequency $\bar{\nu} = 6.1$ GHz corresponds to a relaxation time $\tau = (2\pi\nu)^{-1} = 2.61 \times 10^{-11}$ s. This point is plotted in the

relaxation map *Figure 7* as a cross. The other data are taken from literature[3]. The different molecular weight is of no concern, because it only affects very slow processes. The high frequency part is obtained from the damping of surface acoustic waves observed by impulsive surface scattering (ISS). The medium frequencies represent the thermal expansion answer from the same experiment. The lowest frequencies are from PCS. The small offset in $Q_M(+0.015)$ which is found in the region of no dispersion is due to a small difference (+0.007) between the refractive index measured by Brillouin spectroscopy and by an Abbé refractometer.

We now fit the Q_M-function using the VFT law (equation (19)) to describe the temperature dependence of the relaxation time and the $\alpha\beta$-relaxator (equation (16)) for the frequency-dependence of the modulus. This is given as a solid line in *Figure 6*. The relaxation process shows a relaxation step $\Delta M/M_0 = 0.74$, a relaxation time $\tau_0 = 3.72 \times 10^{-15}$ s and an activation energy $U_0 = 22.5\,\mathrm{kJ\,mol^{-1}}$. The Vogel temperature must be set to $T^* = 0$ because fitting T^* leads to an unphysical negative value. The same happens with a Cole–Cole or Davidson–Cole relaxation function resulting in $\alpha > 1$ and $\beta > 1$. Therefore no broadening of the relaxation process must be taken into account. A Debye process yields the correct description. At the low temperature side (higher frequencies) a further process ($T \approx 260\,\mathrm{K}$) is indicated by a small hump. At the high temperature side (lower frequencies) the experimental data exceed the fitting curve, pointing to another phenomenon within this melt, which will be more closely analysed with *n*-alkane melts[14,29].

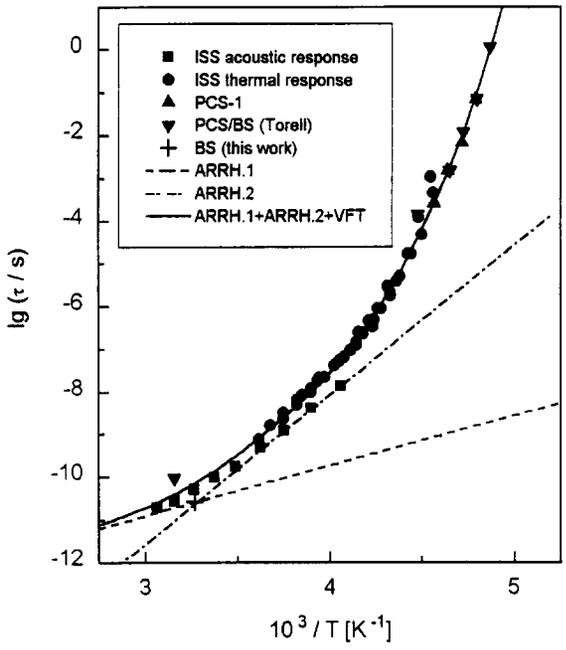

Figure 7 Relaxation map of PPG: +, BS-data (this work), ■ ● ▲ ▼, data taken from literature[3,5]. The relaxation process observed at Brillouin frequencies shows an Arrhenius behaviour (ARRH.1: – – –). The ISS-data from acoustic response (■) fit a sum of two Arrhenius processes (ARRH.2: – · – · –), see also *Figure 8*. The remaining data can be described by the two Arrhenius processes plus an additional Vogel–Fulcher–Tammann law (ARRH.1 + ARRH.2 + VFT: ——)

DISCUSSION

Our analysis clearly reveals a single relaxation behaviour at Brillouin frequencies. The Debye relaxation function just fits the experimental data and no wider process is allowed. The Vogel temperature is unambiguously determined as $T^* = 0\,\mathrm{K}$, the value of a single relaxator. It remains unclear why the other investigators[4,5] arrived at different results. We believe there are two possible reasons:

(i) From the literature, it remains doubtful whether the samples had a controlled water content compare the results on PPG-salt complexes[30].

(ii) An important principal problem is the transformation of measured data to relaxation representations like the reduced modulus given by[5]:

$$N'(\omega) = \frac{M'(\omega) - M_0(\omega)}{M_\infty(\omega) - M_0(\omega)} = \frac{v^2(\omega) - v_0^2(\omega)}{v_\infty^2(\omega) - v_0^2(\omega)}$$

$$N''(\omega) = \frac{M''(\omega)}{M_\infty(\omega) - M_0(\omega)} = \frac{2\alpha(\omega)v^3(\omega)}{\omega[v_\infty^2(\omega) - v_0^2(\omega)]} \quad (22)$$

where the inaccuracy of the line width measurements as well as the assumption that all the broadening observed is due to the viscoelastic damping process introducing errors. A difficulty is the choice of M_0 and M_∞. The former is determined by a linear fit to the high temperature wing of $M'(T)$ and depends on the temperature range covered being correlated to the frequency range via the selected scattering geometry. If the dispersion region is not completely covered by the temperature range for the given scattering geometry this also leads to an incorrect value of M_0. ω and T are not independent variables of $M'(\omega, T)$ but are related by the temperature–frequency superposition principle (equation (17)).

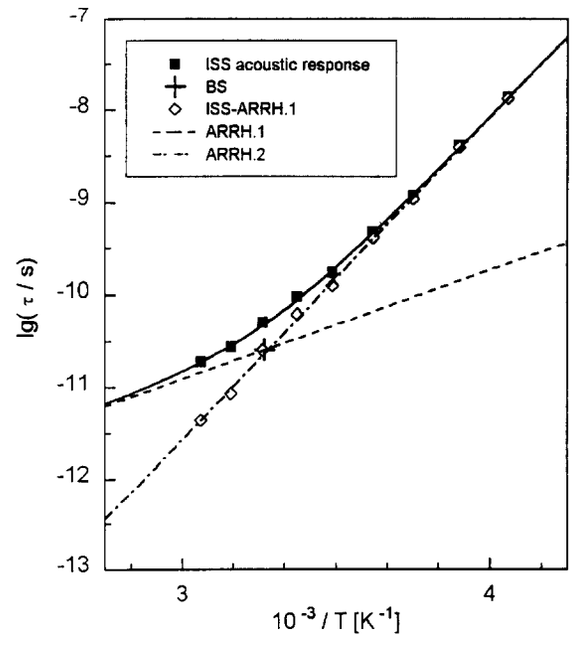

Figure 8 Relaxation map of PPG: subtracting the Arrhenius process observed at Brillouin frequencies (ARRH.1: – – –) from the acoustic part of the ISS measurements (■) yield data with an excellent linear correlation (□). A second Arrhenius process (ARRH.2: – · – · –) becomes obvious

Therefore evaluating M_0 from $M'(T)$ is only correct in the region where $M'(\omega, T)$ is independent from frequency, otherwise the data must first be normalized to a reference temperature. Our data show that even at 400 K there is still a slope in $M'(\omega)$. M_∞ is even harder to obtain and degenerates to an adjustable parameter, if the scanned temperature–frequency window has been selected too small on the low temperature wing. At least some authors are very unhappy with this situation[3]. Again our data show that $M'(\omega)$ still has a slope.

The Q_M-function does not contain these parameters. Since it is the experimentally determined logarithmic derivative we can give one relaxation data point (cross in *Figure 7* and *Figure 8*) without recourse to any model. Invoking a model allows to determination of its parameters as we did with the $\alpha\beta$-relaxation combined with the VFT law (Debye relaxation, dashed line in *Figure 7* and *Figure 8*). If a narrow relaxation process is found the loss modulus follows by equation (15).

It is interesting to explore the sensitivity of the parameters obtained. One of the conclusions in the literature[3,5] is $\beta = 0.4$ as the exponent of the Kohlrausch–Williams–Watts relaxation function

$$\phi(t) = e^{-(t/\tau)^\beta} \tag{23}$$

where τ is the relaxation time and β $(0 < \beta \leqslant 1)$ is a measure of the width of the relaxation time distribution.

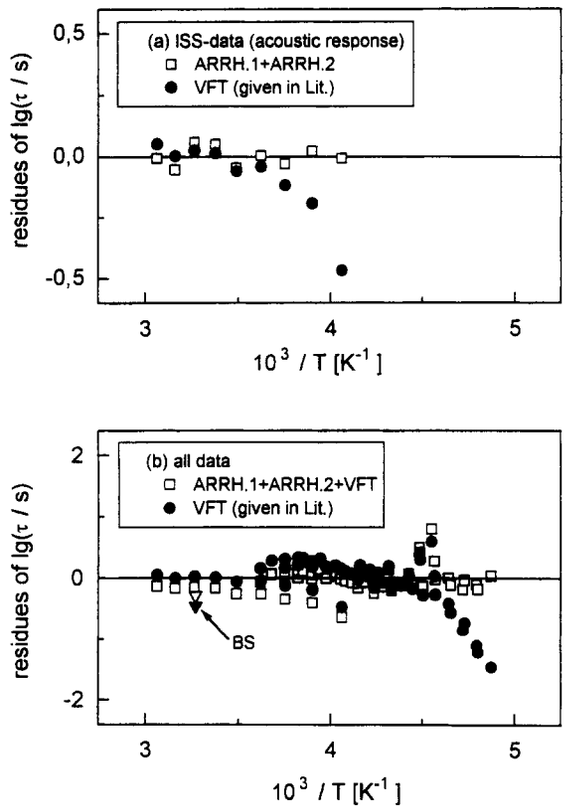

Figure 9 (a) Deviation of the ISS data (acoustic response) from the sum of the Arrhenius processes ARRH.1 and ARRH.2. For comparison the deviation from the VFT law given in reference 3 is shown. (b) Deviation of all data from the sum of the two Arrhenius processes plus an additional VFT process, also compared with the VFT law given in reference 3

The limit $\beta = 1$ is the Debye case with a single relaxation time. $\beta = 0.4$, however, has been fixed for the further treatment resulting for example in a VFT behaviour. This appears questionable even from the published data. In *Figure 7* one can easily draw a straight line fitting the first five data points even better than the VFT curve with $T^* = 176\,K$. Thus an Arrhenius behaviour is more probable. The discussion is much facilitated by knowing the fastest process $\phi_F(t)$ which we subtract from the other data.

$$\phi(t) = \sum_i \phi_i(t) = \phi_F(t) + \phi_R(t) \tag{24}$$

After subtraction of $\phi_F(t)$ the data obtained from the acoustic part of ISS exhibit an excellent linear behaviour (*Figure 8*) revealing a second Arrhenius process, with our data point just on it. The deviations of these ISS-data from the sum of the two Arrhenius processes are plotted in *Figure 9a*.

By lumping together the ISS-data from the thermal expansion and the PCS-data and subtracting now the Arrhenius processes we arrive at a clearly non Arrhenius behaviour. In fitting these data without prejustice we tried different functions: two exponentials, one exponential and one VFT function and finally a single VFT function. All fits are equivalent, as is obvious from the residues. Thus other criteria have to be invoked. One is Occams razor, not to use more explanations than necessary. The second is the physical interpretation of the parameters resulting from the fit. Activation energies of 90 kJ mol^{-1} and 186 kJ mol^{-1} obtained with the two exponentials cannot be understood without chemical processes. The single VFT function remains as the most probable physical fit to the residual data values (*Figure 9b*). With a Vogel temperature $T^* = 161$ K and an activation energy $U_0 = 13.1$ kJ mol^{-1} it is likely to attribute this process to the conformational motions of the main chain leading to the glass process at 190 K. The fast Arrhenius process with an activation energy of 22.5 kJ mol^{-1} seen in the BS and ISS experiments could be attributed to hydrogen bonds of the terminal alcohol groups. Hydrogen bonds have typical energies of 20–50 kJ mol^{-1} [31]. During bond fluctuations this energy acts as activation energy. The low relaxation strength $\Delta M/M_0$ compared to those of primary glass processes is in favour of only a few relaxators operative (Boltzmann factor) or a weak coupling to the sound wave. The appearance of this relaxation independent of molecular weight[4] points to its local character. A chain end effect should decrease, proportional to $1/M_W$. Thus experiments with a PPG of different molecular weight as well as with blocked terminal groups could decide whether our explanation is true or not. The slow Arrhenius process seen in the ISS experiment has a rather high activation energy of 66.9 kJ mol^{-1} but also a high relaxation strength. Hydrogen bonding of water to the chain oxygen groups, e.g. linking two of them by one or two water molecules (two or three hydrogen bonds), requires such energies, and explains the cooperative character inherent in the VFT law. The very short relaxation time τ_0 (*Table 1*) produces at the boiling temperature of water a relaxation time of 2×10^{-13} s comparable to the O–H stretching vibration, which makes sense. The absence of mechanical relaxations in water at room temperature up to Brillouin frequencies has been proven[23]. Thus such processes must

Table 1 Parameters of the relaxation functions used for fitting the data. The last column shows the values of the single VFT behaviour given in reference 3

	ARRH.1	ARRH.2	VFT	VFT (Lit.)
τ_0 (s)	3.72×10^{-15}	8.91×10^{-23}	4.67×10^{-16}	1.83×10^{-14}
U_0 (kJ mol^{-1})	22.5	66.9	13.1	8.5
A (K)	2706	8046	1570	1026
T^* (K)	0	0	161	176

be very fast. Our explanation could be tested by chemical variation of the molecule. The controversial discussion in literature only invokes one average activation energy, 14.7 kJ mol^{-1} (ref. 4) and 21.8 kJ mol^{-1} (ref. 5), lying in the general range of conformational changes and no relation to the special molecular structure of PPG is possible. The conclusion that even at Brillouin frequencies the relaxation time distribution does not narrow[5] is questionable. In fact it narrows to a single relaxation time at about 300 K.

The line width measurements show a broader distribution than the relaxation process allows. A line broadening does not necessarily originate from a dissipation process. Rayleigh scattering of the acoustic wave causes lifetime broadening. We have observed an intense optical Rayleigh scattering around $T = 300$ K. The associated density fluctuation will scatter the acoustic waves as well since the wavelength of light wave and sound wave involved differ at most by a factor of two. The fluctuations mentioned could be due to homophasic (or less probable heterophasic) fluctuations of a crystallization tendency which is finally hindered by the water content. For linear homopolymers $T_M \approx 3/2 \times T_g$ holds and a hypothetic melting temperature $T_M \approx 285$ K results which nicely matches our observations.

After the discussion of the activation energies the question remains whether the experiments are able to sense the same processes. Dielectric measurements couple to the dynamics of permanent dipoles being part of the main chain or of side groups. No wave vector selection is carried out. Thus the processes observed can be local or global. These results have been attributed to the main chain dynamics and coincide with the slow PCS data[5].

PCS records fluctuations of the dielectric tensor. They may be due to molecular motions of anisotropic molecules contributing to the VH scattering. In this case they couple to the main chain conformational dynamics. The VV scattering couples to diffusive density fluctuations of fixed wave vectors and to any kind of dust. The above mentioned phase fluctuations must have strong influence. The main chain dynamics by chain stretching involved in such a process will also be seen by dielectric measurements. In BS propagating density fluctuations of constant wave vector are observed, i.e. sound waves. All activated processes coupling sufficiently fast to density changes will dampen the sound wave. Phase fluctuations scatter sound waves without damping. Their relaxation time is too long to be seen at Brillouin frequencies. In the ISS experiment the fluctuations observed are at first induced. So far it differs from all the other techniques. At first the laser pulse generates a standing energy fluctuation subsequently decaying into different channels. Additionally to normal damping the acoustic wave launched will couple to those induced by thermal density fluctuations since they are existing congruently. The energy stored by broken hydrogen bonds will be dissipated with a much faster time constant than the temperature wave decaying by thermal diffusivity (the thermal expansion signal). Thus, we understand why the ISS experiment senses two Arrhenius processes followed by a slow thermal process, whereas BS only senses the pure acoustic process.

CONCLUSIONS

As relaxation time distribution in PPG we find a set of three different processes, two of which exhibit Arrhenius behaviour and one with Vogel–Fulcher–Tammann behaviour. At high frequencies the relaxation time distribution narrows to a single relaxation time with Arrhenius behaviour. The VFT processes are too slow to influence the measurements at frequencies/temperatures where the Arrhenius processes are prevalent. Our method of using two scattering geometries simultaneously and analysing the data by the Q_M-function is able to unambiguously characterize the dominant high frequency process. In the light of this treatment the use of linewidth results from BS experiments in order to determine the width of the relaxation process becomes questionable. From the present work we believe the experiments with surface acoustic waves to be the most effective, all the more as they can be coupled with BS experiments. In assigning the respective relaxation processes found to corresponding molecular processes, great care must be taken.

ACKNOWLEDGEMENTS

We thank J. K. Krüger for numerous animated discussions. This work was kindly supported by the Deutsche Forschungsgemeinschaft (SFB 239).

REFERENCES

1 Fytas, G., Wang, C. H., Meier, G. and Fischer, E. W. *Macromolecules* 1985, **18,** 1492
2 Alig, I., Stieber, F., Wartewig, S. and Fytas, G. *Polymer* 1988, **29,** 975
3 Duggal, A. R. and Nelson, K. A. *Polym. Commun.* 1991, **32,** 356
4 Wang, C. H. and Huang, Y. Y. *J. Chem. Phys.* 1976, **64,** 4847
5 Börjesson, L., Stevens, J. R. and Torell, L. M. *Polymer* 1987, **28,** 1803
6 Soltwisch, M., Sukmanowski, J. and Quitmann, D. J. *J. Chem. Phys.* 1987, **86,** 3207
7 Oh, T. G., Fischer, E. W., Hellmann, G. P., Russell, T. P. and Wang, C. H. *Polymer* 1986, **27,** 261
8 Krüger, J. K. and Pietralla, M. 'Evidence for Transition-Like

Phenomena in Oligomers and Polymers above their Melt Transition, in Order in the Amorphous "State" of Polymers' (Eds S. E. Keinath, R. L. Miller and J. K. Rieke), Plenum Press, New York, 1987
9 Patterson, G. D., Carroll, P. J. and Pearson, D. S. *J. Chem. Soc., Faraday Trans.* 1983, 2 **79,** 677
10 Krüger, J. K., Marx, A., Peetz, L., Roberts, R. and Unruh, H.-G. *Coll. Polym. Sci.* 1986, **264,** 403
11 Ngai, K. L., Rendell, R. W. and Wang, C. H. *Polymer* 1989, **30,** 369
12 Börjesson, L., Torell, L. M. and Stevens, J. R. *Polymer* 1989, **30,** 370
13 Krüger, J. K. in 'Brillouin Spectroscopy and its Application to Polymers, in Studies in Polymer Science 5—Optical Techniques to Characterize Polymer Systems' (Ed. H. Bässler), Elsevier Science Publishers, Amsterdam, 1989
14 Krbecek, H. H. 'Untersuchung der elastischen Eigenschaften anisotroper Polymere im Hyperschallbereich mit Hilfe hochauflösender Brillouinspektroskopie', Shaker-Verlag, Aachen, 1994
15 Peetz, L. Ph.D.thesis, Saarbrücken (1987)
16 Smith Jr., K. J. In 'Polymer Science I' (Ed. A. D. Jenkins), North-Holland Publishing Company, Amsterdam, 1972
17 Havriliak, S. and Negami, S. *J. Polym. Sci.* 1966, **C14,** 99
18 Cole, K. S. and Cole, R. H. *J. Chem. Phys.* 1941, **9,** 341
19 Davidson, D. W. and Cole, R. H. *J. Chem. Phys.* 1951, **19,** 1484
20 Williams, M. L., Landel, R. F. and Ferry, J. D. *J. Am. Chem. Soc.* 1955, **77,** 3701
21 Huang, Y. Y. and Wang, C. H. *J. Chem. Phys.* 1975, **62,** 120
22 Weeger, R. M. Ulm (1986)
23 Ostwald, J., Pazold, W. and Weis, O. *Appl. Phys.* 1977, **13,** 351
24 Landolt, H. and Börnstein, F. R. Neue Serie II/5—Molekularakustik, Springer-Verlag, Berlin, 1967
25 Greenspan, M. and Tschiegg, C. *J. Acoust. Soc. Am.* 1959, **31,** 75
26 D'Ans Lax, 'Taschenbuch für Chemiker und Physiker I, 3', revised edition, Springer-Verlag, Berlin, 1967
27 Born, M. and Wolf, E. 'Principles of Optics, 3', revised edition, Pergamon Press, Oxford, 1965
28 Engeln-Müllges, G. and Reutter, F. 'Formelsammlung zur numerischen Mathematik mit C-Programmen', Wissenschaftsverlag, Mannheim, 1987
29 Krbecek, H. H. and Pietralla, M. to be published
30 Schantz, S., Torell, L. M. and Stevens, J. R. *J. Chem. Phys.* 1991, **94,** 6862
31 Siesler, H. W. and Holland-Moritz, K. 'Infrared and Raman Spectroscopy of Polymers', Marcel Dekker Inc., New York, 1980